ACSNANO

www.acsnano.org

ARTICLE

# Holographic Optical Tweezers and Boosting Upconversion Luminescent Resonance Energy Transfer Combined Clustered Regularly Interspaced Short Palindromic Repeats (CRISPR)/Cas12a Biosensors

Cheng-Yu Li,* Bei Zheng, Jiang-Tao Li, Jia-ling Gao, Yu-Heng Liu, Dai-Wen Pang, and Hong-Wu Tang*

Cite This: https://dx.doi.org/10.1021/acsnano.0c09986

Read Online

ACCESS | Metrics & More | Article Recommendations | Supporting Information

**ABSTRACT:** Taking advantage of outstanding precision in target recognition and *trans*-cleavage ability, the recently discovered CRISPR/Cas12a system provides an alternative opportunity for designing fluorescence biosensors. To fully exploit the analytical potential, we introduce here some meaningful concepts. First, the collateral cleavage of CRISPR/Cas12a is efficiently activated in a functional DNA regulation manner and the bottleneck which largely applicable to nucleic acids detection is broken. After selection of a representative aptamer and DNAzyme as the transduction pathways, the sensing coverage is extended to a small organic compound (ATP) and a metal ion ($Na^+$). The assay sensitivity is significantly improved by utilizing a bead-supported enrichment strategy wherein emerging holographic optical tweezers are used to enhance imaging stability and simultaneously achieve multiflux analysis. Last, a sandwich-structured energy-concentrating upconversion nanoparticle triggered boosting luminescent resonance energy transfer mode is comined to face with complicated biological samples by skillfully confining the emitters into a very limited inner shell. Following the above attempts, the developed CRISPR/Cas12a biosensors not only present an ultrasensitive assay behavior toward these model non-nucleic acid analytes but also can serve as a formidable toolbox for determining real samples including single cell lysates and human plasma, proving a good practical application capacity.

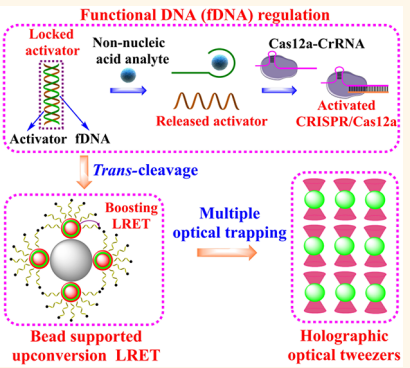


**KEYWORDS:** *optical tweezers, upconversion luminescence, CRISPR, biosensor, functional DNA*

Currently, a revolutionary gene editing technology based on clustered regularly interspaced short palindromic repeats (CRISPR) has aroused widespread attention in analytical science.[1−12] This well-known "genetic scissor" is inspired by the employment of RNA-guided (CrRNA) nucleases (Cas enzymes) in bacteria and archaea to degrade the genome of an invading virus, and such an adaptive immunity pattern makes it possible to artificially engineer the endogenous gene of any species.[13] In practice, owing to the strict complementarity-dependent cleavage principle, the CRISPR/Cas systems have very high precision in the recognition of target nucleic acids, and thus, they are exploited as an efficient tool for developing a wealth of biosensors in fluorescent,[1−3,10−12] electrochemical,[4,5] and colorimetric[6−9] platforms to further enhance accuracy. In addition, these systems can also act as an alternative actuator to generate the signal.[14] However, because of the lack of sufficient analyte transduction pathways to fulfill the activation of CRISPR/Cas, almost all of the present biosensors can only meet the requirements of nucleic acid detection. Therefore, seeking other means to extend the sensing coverage such as some vital small molecules to strengthen the application range is of enormous importance.

Among the available Cas family, a most recently discovered Cas12a enzyme (a class of type V nuclease) can not only initiate the programmed target DNA cleavage process (termed as *cis*-cleavage) like the widely applied Cas9 enzyme but also indistinguishably cleave an additional nonspecific single-

Received: November 28, 2020
Accepted: January 6, 2021

**Scheme 1. Workflow (Not to Real Scale) and Sensing Principle of CRISPR/Cas12a Biosensor under Functional DNA Regulation for the Transduction of Non-Nucleic Acid Analytes by Combining Holographic Optical Tweezers with an Energy-Concentrating UCNP-Triggered Boosting Upcoversion LRET**

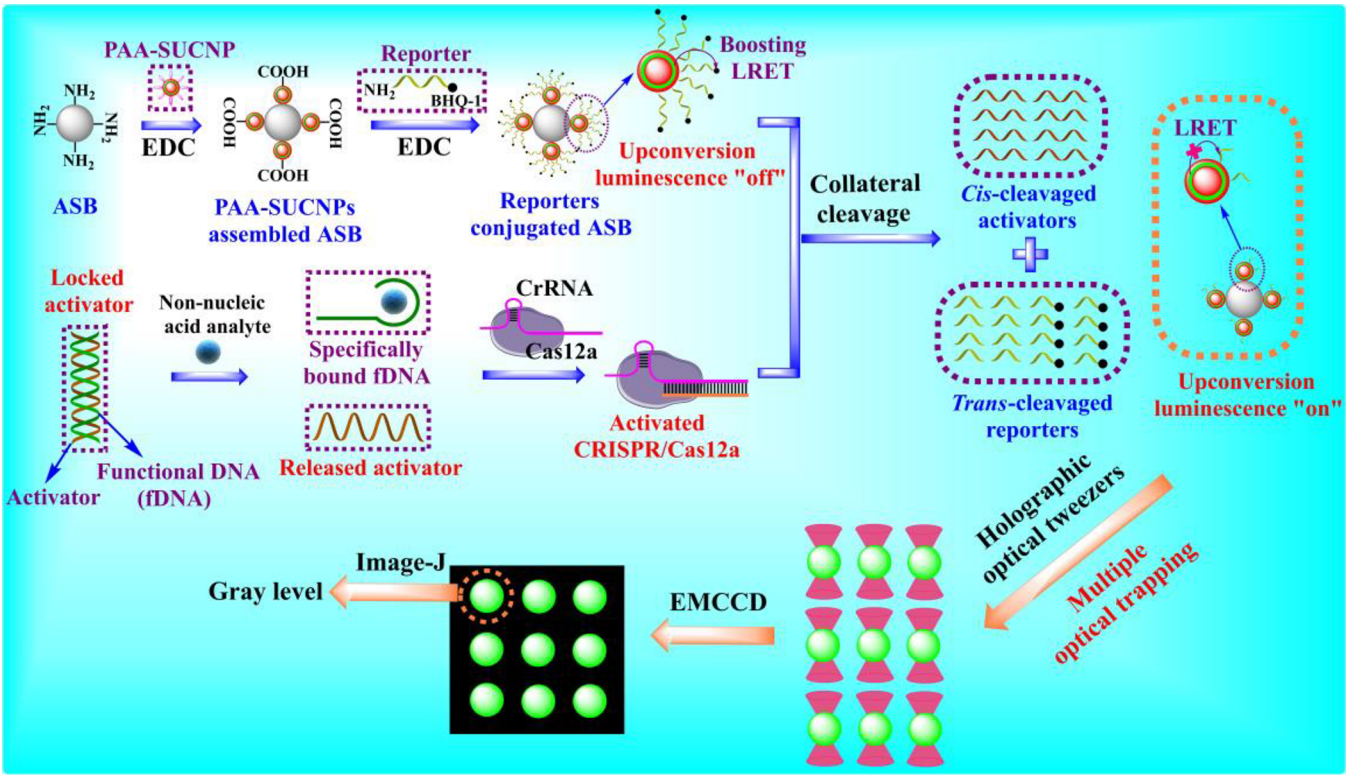


stranded DNA reporter (termed as *trans*-cleavage).[15,16] By virtue of the particular collateral cleavage, the transduction model becomes more convenient and flexible, especially integrating this advanced concept into fluorescence assay and further combining a functional DNA-based transduction pathway.[11] Although some progress has been made regarding fluorescence-based CRISPR/Cas12a biosensors, most of them are carried out in homogeneous solutions without using any auxiliary interfaces to enrich the target analytes, compelling them very difficult to improve sensitivity. In comparison with the conventional solid-phase plane, the bead interface has a negligible surface difference and its three-dimensional structure offers better biomolecular binding efficiency.[17−19] Thus, utilizing the bead to support the CRISPR/Cas12a system is an ideal option to promote its sensing performance.

For bead-supported fluorescence analysis, fluorescent materials and signal acquisition instruments are the two key points. For the former, the frequently used fluorophores including quantum dots and organic dyes are normally excited by visible-light sources. Ascribing to the interference of spontaneous background signals, this general Stokes emission can hardly provide effective optical information in complicated biological samples.[20] Reassuringly, another choice, upconversion luminescence nanoparticle (UCNP), is promising to conquer this problem. In bioassays, the special converting ability toward near-infrared (NIR) photons can perfectly produce an optically transparent window to ensure a superior signal-to-background (S/B) ratio.[21,22] Furthermore, UCNP is able to be served as a hopeful energy donor to construct luminescent resonance energy transfer (LRET) mode with other fluorescent or quenching substances to further avoid false signals.[23−27] However, the larger size of UCNP (typically over 20 nm) allows these energy acceptors to only receive the transferred energy near the surface luminescence, while many internal emitters are mostly ineffective donors, leading to a poor LRET efficiency (usually less than 50%). Hence, exploring a strategy to rationally modify the structure of UCNP to control the luminescence domain at the optimal LRET distance demand (<10 nm) is of necessity. Until now, a feasible notion that is the use of a very thin shell to concentrate the upconversion luminescence energy is an effective solving way.[28,29]

For the latter, fluorescence microscope is usually selected to collect optical signals because of its intuitive image output form. But in actual operation, beads are suspended in aqueous environments, and thus, the fluid viscous force is very likely to affect such a nonstatic state.[30,31] The most common situation is that the beads may well deviate from the focal plane and the fluctuation of excitation conditions cannot afford reliable results even with user intervention such as refocusing. Fortunately, with the rapid development of optical science, an exciting optical manipulation concept named optical tweezers can well surmount this imaging uncertainty.[32−35] In principle, the gradient force generated by a tightly focused Gaussian-shaped laser beam is in the order of pN and this is a very good range of mechanics to neutralize the fluid impact. Although the introduction of optical tweezers into microscope can significantly enhance the imaging stability, the traditional optical tweezers are referred as a single beam potential well and their limited trapping behaviors (trapping one bead at a time) renders a challenge in conducting high-throughput detection. To promote the trapping flux, another emerging holographic technique incorporated optical trapping (termed as holographic optical tweezers) shows huge prospect to actualize this goal.[36,37]


https://dx.doi.org/10.1021/acsnano.0c09986
*ACS Nano* XXXX, XXX, XXX−XXX

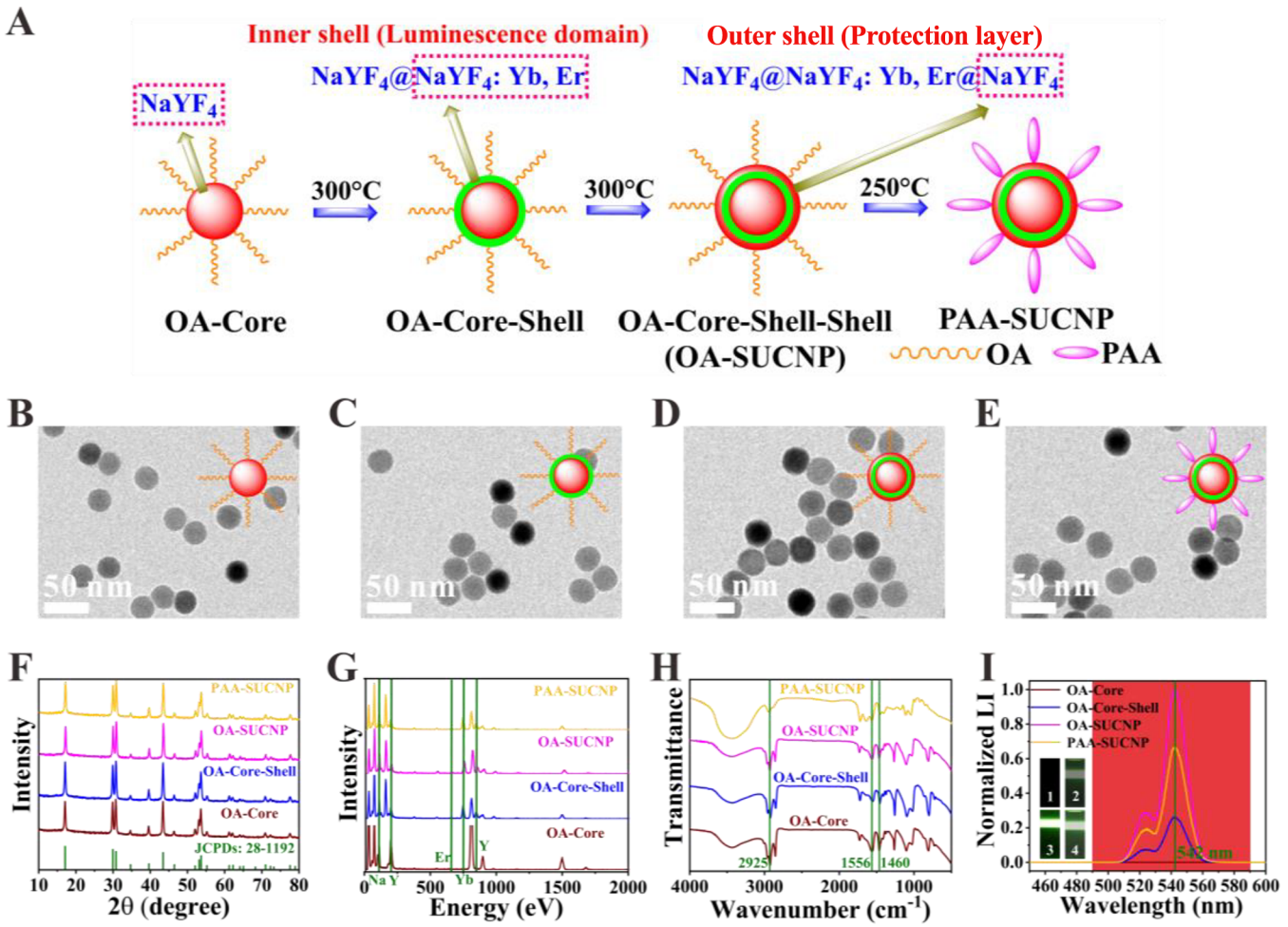


**Figure 1. (A) Development path of sandwich-structured energy-concentrating UCNP coated with oleic acid (OA) *via* a layer-by-layer based seed-mediated growth at 300 °C and its surface PAA modification through a ligand-exchange route at 250 °C (not to real scale). (B−E) TEM images (scale bars are 50 nm) of $NaYF_4$ (OA-core), $NaYF_4$@$NaYF_4$: Yb, Er (OA-core−shell), $NaYF_4$@$NaYF_4$: Yb, Er@$NaYF_4$ (OA-SUCNP), and PAA-SUCNP. (F−H) XRD patterns, EDS lines, and FT-IR spectra of nanoparticles from (B)-(E). (I) Upconversion luminescence spectra of synthesized nanomaterials dispersed in corresponding solvents. Red region: signal acquisition region in detection process. Inset: using a 980 nm portable laser to irradiate these solvents (laser powers are 500 mW). OA-core, OA-core−shell, and OA-SUCNP in chloroform are presented as numbers 1−3, respectively, and PAA-SUCNP in ultrapure water is presented as number 4. Concentrations are ∼10 mg/mL for all cases.**

Encouraged by the challenges above, we herein bring forward a functional DNA (fDNA) regulated CRISPR/Cas12a biosensor by combining holographic optical tweezers with an energy-concentrating UCNP triggered boosting LRET and employ it to achieve the transduction of non-nucleic acid analytes. Scheme 1 illustrates the main parts of this biosensor: (i) using a poly(acrylic acid) (PAA) modified sandwich structured UCNP (SUCNP) to construct a boosting LRET mode on a supporting bead; (ii) designing a peculiar CRISPR/Cas12a system activated by fDNA programmed regulation; (iii) performing *trans*-cleavage process toward the reporters on bead surface; and (iv) collecting upconversion luminescence under multiple optical trapping. On one hand, PAA-SCUNPs are first covalently assembled onto the surface of an amino-modified silica bead (ASB) and the PAA-SUCNPs assembled ASB is then conjugated with the reporters modified with amino and BHQ-1 at both ends (an extremely short single stranded DNA with 5 nt). For this reporter-conjugated ASB, the upconversion luminescence is intensively quenched by reason for the very closing space distance between the luminescence domain (the inner shell of SUCNP) and the BHQ-1 molecules. On the other hand, the activator is first locked by hybridizing with a fDNA and then it is released from the blocking structure upon the fDNA specifically bound with a non-nucleic acid analyte. When a CrRNA-Cas12a complex recognize the released activator, the upconversion luminescence will be restored due to the programmed collateral cleave of CRISPR/Cas12a system. Under holographic optical tweezers, a 3 × 3 bead array formed by multiple optical trapping is captured by an electron-multiplying CCD (EMCCD) and finally the gray levels are counted to conduct quantitative determination.

## RESULTS AND DISCUSSION

**Fabrication and Characterization of Energy-Concentrating UCNP.** In order to construct an exceptional energy-concentrating UCNP, a conventional seed-mediated growth regulation[38] is employed to achieve an oleic acid (OA) coated sandwich structure comprising a core and inner/outer shells (Figure 1A). With regard to this incremental synthetic pathway, an environmentally friendly thermal decomposition strategy using rare earth chlorides as the precursors at high temperature (300 °C) is exploited to create each hydrophobic layer. In particular, a pure $NaYF_4$ host matrix is first fabricated as the core


https://dx.doi.org/10.1021/acsnano.0c09986
ACS Nano XXXX, XXX, XXX−XXX

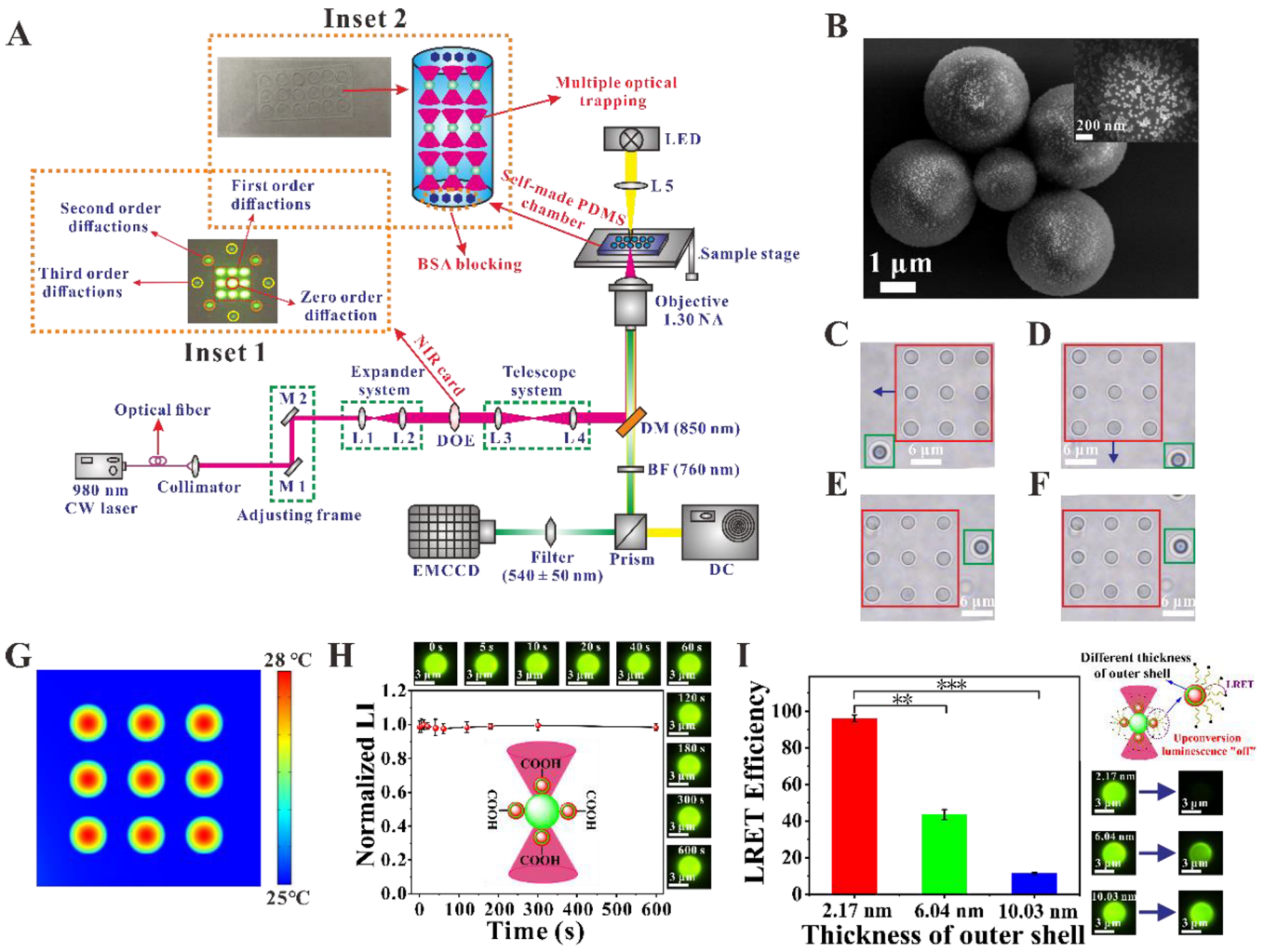


**Figure 2. (A) Schematic diagram of self-established holographic optical tweezers instrument. Abbreviations: M = mirror, L = lens. Focal lengths of L1−L4 are 25, 75, 150, and 150 mm, respectively. Inset 1: corresponding diffractions projected onto an NIR card. Inset 2: self-made PDMS chamber. Light red line: optical path of 980 nm laser beam. Green line: upconversion luminescence path. Yellow line: illumination path of LED lamp. (B) SEM image (scale bar is 1 $\mu$m) of PAA-SUCNPs assembled ASBs. Inset: magnified area (scale bar is 200 nm) of a representative single assembled bead. (C−E) Optical manipulation of 3 × 3 bead array (trapping pure ASB) in horizontal direction *via* a passive approach (moving sample stage). (F) Optical manipulation of bead array from (E) in axial direction *via* an active approach (adjusting objective). Red and green boxes represent a 3 × 3 bead array and referential bead, respectively, and the blue arrow indicates manipulation path. Scale bars are 6 $\mu$m for all cases, and these images are recorded by a DC. (G) Finite element simulation of the horizontal temperature profile around 3 × 3 focal points using COMSOL Multiphysics software. (H) Investigation of luminescence stability by optically trapping a single PAA-SUCNPs assembled bead. (I) Inspection of LRET efficiency by optically trapping a single reporters conjugated bead (PAA-SUCNPs with different thickness of outer shells). Scale bars and exposure time are 3 $\mu$m and 400 ms for all cases, respectively. **$P$ < 0.01, ***$P$ < 0.001.**

material alone and then a very thin $NaYF_4$ inner shell (~2 nm) codoped with 18% $Yb^{3+}$ (sensitizer) and 2% $Er^{3+}$ (activator) is developed to confine the luminescence energy. Due to the solvent quenching effect to such a bared luminescence domain, another $NaYF_4$ outer shell are extended as the protection layer. At the liquid−liquid interface (250 °C), the primordial surface OA molecules are finally replaced by low molecular PAA polymers (average MW is ~1.8 Kda) *via* a simple ligand exchange route[39] to prepare a hydrophilic carrier, endowing a commendable candidate for performing the subsequent biological covalent coupling.

A succession of transmission electron microscopy (TEM) images visibly exhibit the morphology and size evolution (Figure 1B−1D), for which the as-adopted shell development manner can well keep all of the nanoparticles in spherelike forms and no agglomerations appear to this crystal-broadening process. It is worth noting that the favorable monodispersity of the sandwich case is not affected by the surface ligand replacement (Figure 1E). Size statistical data within quite narrow ranges ($n$ = 300, $\sigma$ < 6%) precisely reflects the particle increasing of these hydrophobic ones (Figures S1A−S1C), among which the mean diameter of the initial $NaYF_4$ core (OA-core, 24.52 nm) is gradually increased to 26.61 nm ($NaYF_4$@$NaYF_4$: Yb, Er, OA-core−shell) and finally to 28.78 nm ($NaYF_4$@$NaYF_4$: Yb, Er@$NaYF_4$, OA-SUCNP), along with no apparent size variation comes to the PAA modification (28.82 ± 1.39 nm, Figure S1D). High-resolution TEM images prove that highly crystalline properties are presented to all the nanostructures and the spaces between these evident lattice fringes are estimated to be 0.52 nm (Figures S2A−-S2C), indicating the appearance of (100) crystal face for hexagonal direction index. Such conjecture is additionally demonstrated by X-ray diffraction (XRD) patterns (Figure 1F), wherein all cases are single crystals and their characteristic diffraction signals are perfectly in line with the standard peaks of


https://dx.doi.org/10.1021/acsnano.0c09986
ACS Nano XXXX, XXX, XXX−XXX

hexagonal phase $NaYF_4$ (JCPDs: 28−1192), also uncovering the fine control of crystal stability during the layer-by-layer growth. The exact distribution of rare earth elements in each layer is attested by energy-dispersive X-ray spectroscopy (EDS) measurements, by which the pairing sensitizers/activators are definitively distributed in the inner shell (Figure 1G). With the assignment of some typical OA bands at 1460 $cm^{-1}$/1556 $cm^{-1}$ (antisymmetric/symmetric vibration of carboxylate anions) and 2925 $cm^{-1}$ (asymmetrical long alkyl chain stretching) in Fourier transform infrared (FT-IR) spectra, the surface OA coating is certified to be successful (Figure 1H, three bottom lines) and the maintenance of such nonpolar features can bring about excellent chloroform solubilities (transparent solutions at ∼10 mg/mL for all cases, Figure S3A−3C), whereas a marked weakening sign happens to these specific positions when exchanging with the PAA polymers (Figure 1H, top line) and this hydrophilic transformation will lead to a transparent water solution (Figure S3D).

Use of a portable 980 nm continuous wave (CW) laser (output power: 500 mW) to irradiate these solutions shows that the introduction of an outer shell can act as a valid barrier to the surrounding solvent molecules and results in a significant strengthening of the green upconversion luminescence (Figure 1I, insets 1−3). The defined enhancement factor is determined by spectral analysis, whereby the featured maximum emission wavelength at 542 nm stemming from the $Er^{3+}$ transition from energy level $^4S_{3/2}$ to $^4I_{15/2}$ (Figure S4) is 3.68-fold higher than the unprotected core−shell structure (Figure 1I, blue and purple lines). While the effect of nonradiative relaxion in water attenuates the luminescence intensity by about 35% (Figure 1I, orange line and inset 4), the PAA-SUCNP can commendably sustain its colloidal and optical characters (Figure S5) for up to 40 days, ensuring a forceful linking carrier for conjugating biomolecules.

**Establishment of Holographic Optical Tweezers Instrument.** As depicted in Figure 2A, the core technology of our self-established holographic optical tweezers instrument is derived from the use of a diffractive optical element (DOE) to produce multiple potential wells. Concretely, an optical fiber coupled 980 nm CW laser (maximum output power: 950 mW, single-mode light spot, $M^2$ is ∼1.1, Connet, China) equipped with a collimator is operated as the double source for trapping and exciting. The collimated beam with a size of 3 mm first passes through an adjusting frame consisting of two reflectors to actualize axial height regulation and then it is guided into an expander system (1:3), leading to a larger spot size (∼9 mm) capable of properly overfilling the pupil of a 100× oil-immersed objective (Olympus) with a high numerical aperture (NA: 1.30). After proceeding with the DOE to realize phase-modulation, an effective splitting phenomenon occurs to the original single beam and the corresponding zero to third order diffractions can be projected onto a NIR card (Figure 2A, inset 1), in which the zero and first orders form a uniform primary array (3 × 3 spots) while an uneven peripheral subarray is generated by others. Considering the consistency of excitation conditions, the primary spots are selected as the signal detection region. Upon using a telescope system (1:1) to accurately make the trapping plane consistent with the imaging plane, the 3 × 3 beam array is imported into an inverted microscope system holding an infinite optical path (Olympus IX70), followed by reflection upward by its internal dichroic mirror (DM, 850 nm). By tightly focusing these Gaussian-shaped beams on a mobilizable sample stage, a 3 × 3 diffraction limited spot array (∼1 $\mu$m for each focus) is produced into the self-made polydimethylsiloxane (PDMS) chamber (Figure 2A, inset 2) to accomplish the arrayed optical-trapping events. Before collecting the upconversion luminescence ranging from 490 to 590 nm with a cooled EMCCD (Evolve 512 Delta, Photometrics, Canada), it is necessary to eliminate the interference of the residual 980 nm laser by a blocking filter (BF, 760 nm). Beyond that, the bright-field illumination implemented by a slightly converged light-emitting diode (LED) lamp (white light, output power: 3 W) is recorded in real time by a digital camera (DC). Owing to the optical loss of the above components, approximately 40% of the output power can finally reach the focus area.

**Surface Covalent Coupling of ASB.** To guarantee a potent bead supported energy donor, EDC coupling chemistry is then applied to achieve the covalent attachment of amino sites on ASB and carboxyl groups on PAA-SUCNP. A representative scanning electron microscopy (SEM) image distinctly confirm such assembling case, by which a scattered layer of PAA-SUCNPs is evenly covered onto the surface of each bead (Figure 2A). In view of the remaining unactivated carboxyl sites on the assembled PAA-SUCNPs, the amino-modified reporters can be further bound onto the ASB according to the same approach. As anticipated, no significant absorption at 260 nm (a featured location for nucleic acids)[40] appears to the collected reaction supernatant (Figure S6A), suggesting that the energy acceptors are almost entirely conjugated onto the donor surface. Of note, the above series of linking events are also verified by dynamic light scattering results (Figure S6B), where the initial positively charged ASB (+ 12.6 mV) becomes more negative because PAA-SUCNP and DNA molecules are both electronegative, *i.e.*, −10.2 mV and −27.3 mV for PAA-SUCNPs-assembled ASB and reporters conjugated ASB, respectively.

**Calibration of the Home-Built Setup.** Before bringing the as-proposed bead supported LRET assay mode into practical force, the following crucial points need to be calibrated to make the home-built setup work optimally. First, unlike traditional single beam gradient force based optical tweezers, the current holographic pattern shows nine primary split beams. For this reason, investigating whether the divided laser power is robust enough to conduct the expected 3 × 3 trapping is necessary. By progressively adjusting the laser output power, the gradient force for the trapping array can overcome the fluid viscous force unless the output power is greater than 500 mW, under which the formed 3 × 3 bead array (trapping pure ASB) can be easily manipulated in three dimensions (Figures 2C−F). Second, previous reports have proved that UCNP is a sort of temperature-sensitive material and its luminescence nature will observably change when the ambient temperature exceeds 35 °C.[41,42] Therefore, the balance between gradient force and laser local heating effect is another important consideration. As presented in the horizontal temperature simulation data (Figure 2G), the theoretical temperature profile around each focal area is from 25 to 28 °C at 500 mW output power, allowing very suitable thermal conditions (corresponding to ∼22.22 mW at each focal point) for carrying out luminescent signal acquisition. Third, although each trapping spot has sufficient power density (∼2.79 × $10^4$ W/$cm^2$) to ensure the efficient triggering of upconversion luminescence, the optical stability under such harsh excitation is also a concern. To examine this challenge, the luminescence intensity of a single PAA-SUCNPs assembled ASB falling into the trapping array is continuously monitored. Satisfactorily, profiting from the weak photodamage resulting from the NIR source and the excellent resistance of UCNP to


https://dx.doi.org/10.1021/acsnano.0c09986
ACS Nano XXXX, XXX, XXX−XXX

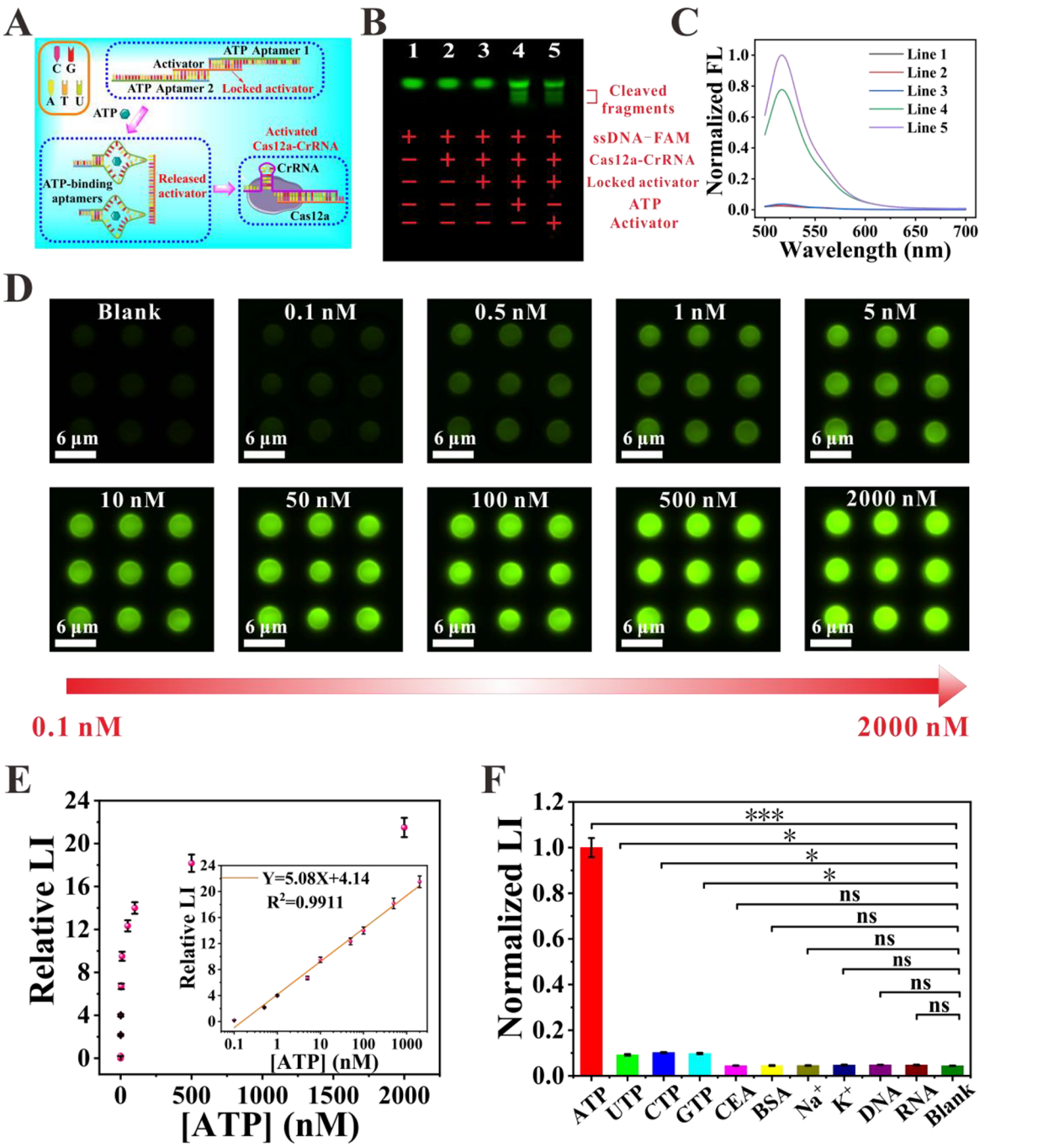


**Figure 3.** (A) Activation principle of CRISPR/Cas12a system under dual ATP aptamers regulation (not to real scale). Due to the combination efficiency of aptamer and the highly efficient multiturnover feature of the CRISPR/Cas12a system, the actual reaction ratio between activator, target, and CrRNA does not follow as the drawing. (B) 3% agarose gel electrophoresis verification of the aptamers regulated CRISPR/Cas12a system toward *trans*-cleaving ssDNA-FAM. (C) Fluorescent analysis of the aptamers regulated CRISPR/Cas12a system toward *trans*-cleaving FAM and BHQ-1 double-modified reporter. Lines 1−5: reporter, Cas12a-CrRNA + reporter, Cas12a-CrRNA + locked activator + reporter, Cas12a-CrRNA + ATP + locked activator + reporter, Cas12a-CrRNA + activator + reporter, respectively. (D) Upconversion luminescence images (false color, scale bars are 6 $\mu$m) of 3 × 3 bead arrays introduced with different amounts of ATP (0.1−2000 nM). Exposure times are 400 ms for all cases. (E) Linear relationship (working curve) between the relative luminescence intensity ($(I - I_0)/I_0$) and the logarithm of [ATP]. Correlation ratios between activator, ATP and CrRNA are from 1:0.00004:0.04 to 1:0.8:0.04. (F) Specificity examination toward UTP, CTP, GTP, CEA, BSA, $Na^+$, $K^+$, DNA and RNA. *$P$ < 0.05, ***$P$ < 0.001, ns: no significant difference ($P$ > 0.05).

photobleaching,[23,24] the measured object entirely displays no indication of signal decay even if the excitation time is maintained for up to 10 min (Figure 2H).

**Inspection of the Optimal LRET Efficiency on ASB.** For this sandwich-structured UCNP design, because the inner shell possesses an ideal space scope (only 2.09 nm) to intensively restrict the luminescent rare earth ions, the growth thickness of outer shell can vastly influence the LRET efficiency to the surface energy acceptors by virtue of the different closing distances. To validate such a deduction, additional batches of OA-SUCNPs with a thicker outer shell are then synthesized by making the core−shell structure stay the same. In accordance


https://dx.doi.org/10.1021/acsnano.0c09986
ACS Nano XXXX, XXX, XXX−XXX

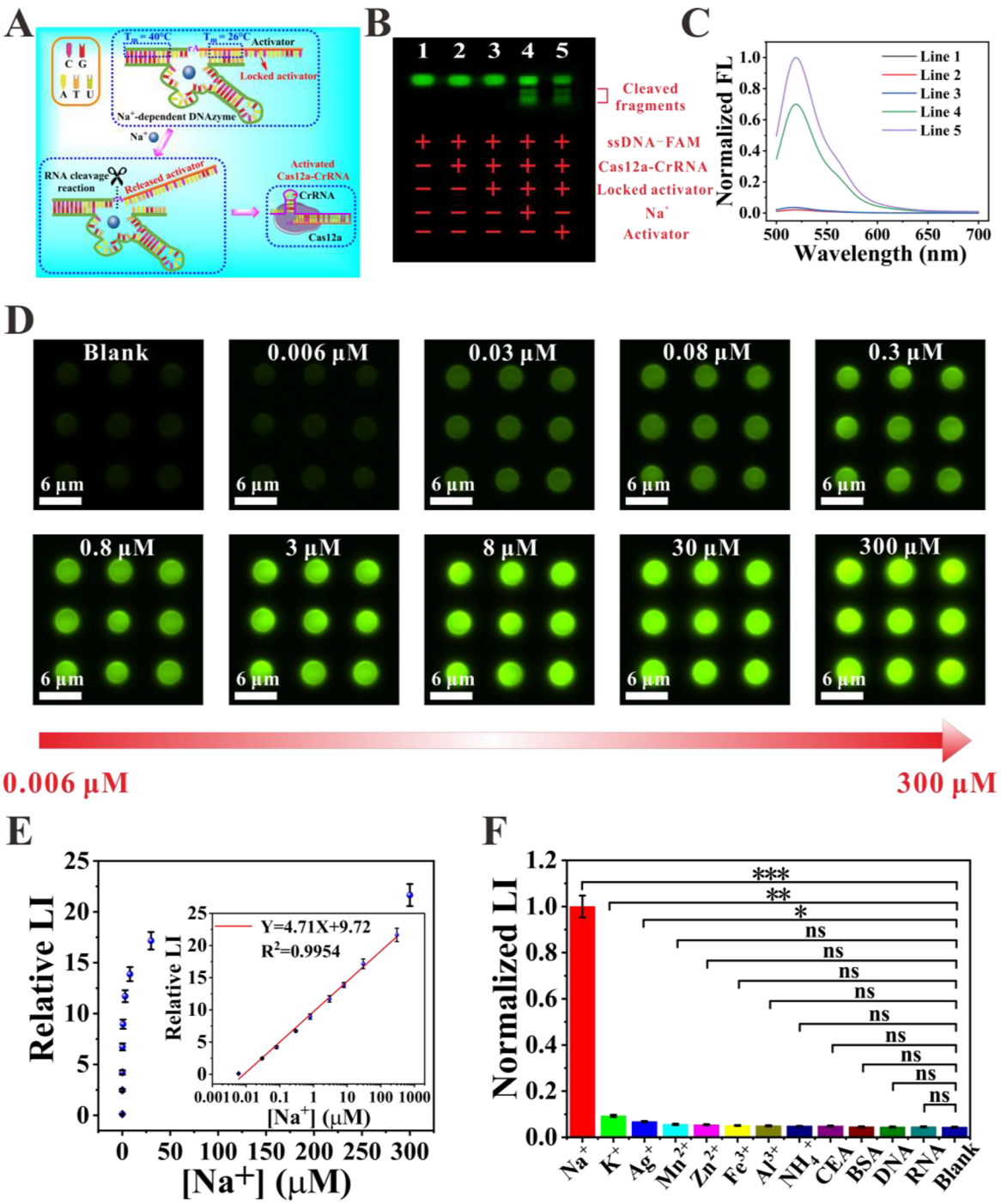


**Figure 4.** (A) Activation principle of CRISPR/Cas12a system under $Na^+$-dependent DNAzyme regulation (not to real scale). Because of the combination efficiency of DNAzyme and the highly efficient multiturnover feature of CRISPR/Cas12a system, the actual reaction ratio between activator, target, and CrRNA does not follow as the drawing. (B) 3% agarose gel electrophoresis verification of the DNAzyme regulated CRISPR/Cas12a system toward *trans*-cleaving ssDNA-FAM. (C) Fluorescent analysis of the DNAzyme regulated CRISPR/Cas12a system toward *trans*-cleaving FAM and BHQ-1 double modified reporter. Lines 1−5: reporter, Cas12a-CrRNA + reporter, Cas12a-CrRNA + locked activator + reporter, Cas12a-CrRNA + $Na^+$ + locked activator + reporter, Cas12a-CrRNA + activator + reporter, respectively. (D) Upconversion luminescence images (false-color, scale bars are 6 $\mu$m) of 3 × 3 bead arrays introduced with different amounts of $Na^+$ (0.006 to 300 $\mu$M). Exposure time are 400 ms for all cases. (E) Linear relationship (working curve) between the relative luminescence intensity $((I - I_0)/I_0)$ and the logarithm of $[Na^+]$. Correlation ratios between activator, $Na^+$, and CrRNA are from 1:0.0012:0.04 to 1:12:0.04. (F) Specificity examination toward $K^+$, $Ag^+$, $Mn^{2+}$, $Zn^{2+}$, $Fe^{3+}$, $Al^{3+}$, $NH^{4+}$, CEA, BSA, DNA, and RNA. *$P$ < 0.05, **$P$ < 0.01, ***$P$ < 0.001, ns: no significant difference ($P$ > 0.05).

with the Ostwald ripening principle, the crystal size can be effectively regulated by varying the amounts of ligands.[43] When altering the OA/1-octadecene (ODE) ratio from 2:5 to 3:4 and 4:3, the outer shells are extended from 2.17 to 6.04 nm (mean diameter: 32.65 nm, Figures S7A,B) and 10.03 nm (mean diameter: 36.64 nm, Figure S7C,D), respectively. It should be pointed out that neither the crystal conformation nor the hydrophobic coating has changed for this size-controlling


https://dx.doi.org/10.1021/acsnano.0c09986
ACS Nano XXXX, XXX, XXX−XXX

process (Figures S8 and S9). After transforming these larger OA-SUCNPs into water-soluble ones (Figures S10), we explore the corresponding energy transfer from the concentrated upconversion luminescence to the surface BHQ-1 molecules by constructing the optical trapping based single bead imaging. It is seen from Figure 2I that the LRET efficiency becomes weaker with the increasing thickness of the outer shell and the very high efficiency for 2.17 nm case (96.1%) is prominently dropped to 43.5% (6.04 nm case) and 11.4% (10.03 nm case), respectively, suggesting a controllable manner to conduct the energy-concentrating notion.

**Quantitative Analysis of Standard ATP.** By means of the above reliable basics, the bead-supported CRISPR/Cas12a sensing approach is put forward for transducing non-nucleic acid analytes with the assistance of fDNA. To begin, the widely studied adenosine 5′-triphosphate (ATP) aptamer[44] is selected as the model fDNA to realize structure-switching. The aptamer regulated principle is illustrated in Figure 3A, where two appropriately prolonged ATP aptamers are first hybridized with the activator through a convenient annealing processing to achieve a blocking effect. On account of the stronger binding affinity to the target compound than the partial base complementation, the aptamers are preferentially in response to ATP and the completely locked activator will be released from the hybridization structure to further specifically recognize and finally activate the Cas12a-CrRNA complex. Agarose gel electrophoresis is then used to corroborate the actual activation effect of such aptamer induced CRISPR/Cas12a system by *trans*- cleaving a single stranded DNA substrate (21 nt) labeled with FAM (ssDNA-FAM). In Figure 3B, very similar to the collateral cleaving ability of pure CRISPR/Cas12a, the substrate is obviously digested into a battery of short fragments only in the presence of ATP while no degradation phenomenon happens to the dual ATP aptamers locked case. To reinforce the finding, a fluorescent study toward a FAM and BHQ-1 double modified ssDNA with 5 nt (acting as the reporter) is next conducted. The comparison of fluorescence intensities shows that the locked activator can hardly restore the quenched FAM emission, while a distinct fluorescence signal is detected for the ATP treated group (Figure 3C).

Following the optimal collateral cleavage reaction (*e.g.*, temperature: 37 °C, pH: 8.0, time: 15 min, Figure S11), the different amounts of ATP-activated CRISPR/Cas12a systems are employed to *trans*-cleave the surface reporters on ASB and then the upconversion luminescence signals are determined by the holographic optical tweezer assisted imaging analysis. It can be acquired from the luminescence images (false-color) of 3 × 3 bead arrays that the brightness of inside beads greatly depends on the ATP concentration (Figure 3D), indicating that the increasing introduction of targets will give rise to a more obvious signal recovery trend. After counting 10 3 × 3 bead images (corresponding to 90 measured beads, assay time is ∼20 min) for each concentration group *via* an Image-J software, a good linear relationship ($R^2$: 0.9911) crossing four orders of concentration (from 0.1 to 2000 nM) between the relative luminescence intensity ($(I - I_0)/I_0$, where $I_0$ and $I$ represent the signal intensity in the absence and presence of ATP, respectively) and the logarithm of [ATP] is demonstrated (Figure 3E). Notably, thanks to the uniformity of reaction interfaces (ASB and UCNP) and the special anti-Stokes luminescence, not only the bead luminescence deviation for each testing case is very small (variable coefficients are less than 5%, Table S1) but also the S/B ratio reaches as high as 28.6. Making use of the $3\sigma_b/k$ criterion (where $\sigma$ is the standard deviation of 11 blank samples and $k$ is the slope of linear curve), the limit of detection (LOD) is dramatically reduced to 87 pM compared to the unsatisfactory LOD (∼500 nM) of commercial ATP kit, and this ultrasensitive behavior also exhibits an overt advantage over other optical methods (Table S2).

Apart from sensitivity verification, specificity is another vital performance indicator because the ATP-related interfering substances are abundant in organisms. Hence, our method is tentatively used for responding to three nucleotide-triphosphate analogues (UTP, CTP, and GTP) competing with ATP, other nonspecific macromolecular compounds such as proteins (CEA and BSA) and nucleic acids (DNA and RNA), as well as metal ions ($Na^+$ and $K^+$). It can be found from Figure 3F that the most pronounced luminescence intensity comes from the ATP group ($P < 0.001$). For the former, benefiting from the good selectivity of aptamer, the potential competitive effect produces only a bit higher signals for the blank group ($P < 0.05$) even though their concentrations are 10-fold that of ATP and the actual intensities take up approximately 10% of the target signal. For the latter two cases, because the four different biomolecules and the two metal ions are almost impossible to specifically bind with the ATP aptamer, the signs of signal recovery (even 50-fold higher than the ATP concentration) exhibit no apparent discrepancy to the target group ($P > 0.05$). Together, these convincing examinations suggest that the analytical methodology has a superior specificity.

**Quantitative Detection of Standard $Na^+$.** Inspired by the successful quantitative analysis of ATP, the universality of this developed sensing concept is next testified by conducting $Na^+$ detection. As displayed in Figure 4A, another model fDNA (a recently discovered $Na^+$-dependent DNAzyme)[45] having a similar enzymatic function is employed to flexibly release the activator. Detailedly, a substrate chain embedding with the activator is first complemented to the two binding arms of DNAzyme through an annealing treatment. When the cofactor ($Na^+$) specifically incorporates into the loop structure, the RNA cleavage effect at the rA position is then initiated (Figure S12A). Due to the melting temperature ($T_m$ = 26 °C) of partially complementary activator is far below the incubation temperature (37 °C), the locked activator will be dissociated from the right binding arm (Figures S12B and S12C) to activate the Cas12a-CrRNA complex. Besides, no strand displacement reaction happens between the CrRNA and the hybridized DNAzyme in the absence of $Na^+$ (Figure S13). Like the ATP analysis, such DNAzyme regulated CRISPR/Cas12a system is verified in turn with the electrophoresis experiment (Figure 4B) and the fluorescence inspection (Figure 4C). Based on the same quantitative determination process, the target concentration reliant signal recovery capability (Figure 4D) is also found to be linearly related to the logarithm of $[Na^+]$ ($R^2$: 0.9954) in the range of 0.006−300 $\mu$M (Figure 4E and Table S3), and the LOD is low to 4.3 nM, an extremely satisfactory sensitivity in contrast to the commonly used $Na^+$ selective meter (LOD is ∼100 $\mu$M) and other $Na^+$ fluorescent sensors (Table S4). Moreover, owing to the specific identification of DNAzyme, both the nontarget metal/nonmetallic ions and other biomolecules cannot in favor of restoring the quenched upconversion luminescence ($P > 0.05$, Figure 4F).

**Analysis of ATP in Single Cell.** As is well-known, ATP is a type of high-energy phosphate compound, and it can serve as the most direct energy source in living organisms.[46−48] For cell metabolism, ATP is also a key signaling indicator for revealing


https://dx.doi.org/10.1021/acsnano.0c09986
ACS Nano XXXX, XXX, XXX−XXX

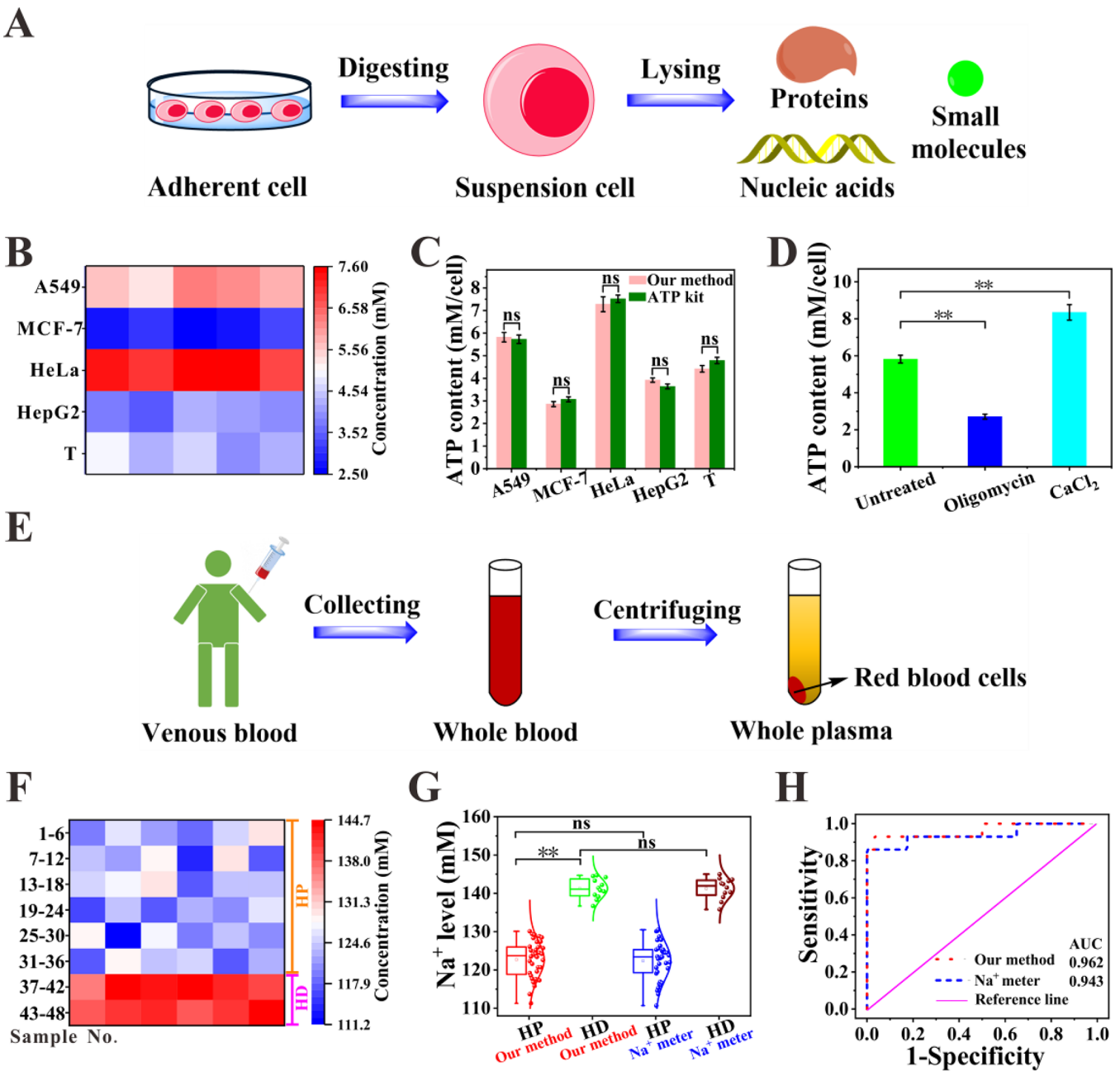


**Figure 5. (A) Extraction procedure of intracellular small molecules. (B) Heat map of ATP contents in single A549, MCF-7, HeLa, HepG2, and T cells. (C) Comparison between commercial colorimetric kit and our method. Ns: no significant difference ($P > 0.05$). (D) *In vitro* monitoring of ATP variation in a single A549 cell after treating with 10 $\mu$M oligomycin (down-regulation reagent) and 5 mM $CaCl_2$ (up-regulation reagent). **$P < 0.01$. (E) Extraction procedure of human whole plasma. (F) Heat map of $Na^+$ levels in 36 cases of hyponatremia patients (HPs) and 12 cases of healthy donors (HDs). (G) Comparison between $Na^+$ meter and our method. **$P < 0.01$, ns: no significant difference ($P > 0.05$). (H) ROC curve of our method and $Na^+$ meter in actual application.**

the activity of various physiological processes from differentiation to apoptosis.[46] Thus, it is very useful to propose an efficient assay strategy to measure this intracellular molecule, especially at the single-cell level. To fulfill this task, our method is finally applied to reflect the ATP contents in five different single cells by taking the advantage of the exciting LOD. Figure 5A presents the extraction procedure of small molecules, for which $10^4$ of adherent cells are first treated with digesting and then dealt with lysing. In light of the ATP concentration window (1−10 mM/cell)[48] and the obtained linear range, the cell lysates need to be diluted thoroughly. The definite ATP content in a single cell is exhibited on the heat map (each kind of cell is measured in five batches, Figure 5B), from which the average ATP content for a single A549, MCF-7, HeLa, HepG2 and T cells are 5.82, 2.86, 7.28, 3.92, and 4.42 mM, respectively, fully agreeing with the data acquired from a colorimetric kit (Figure 5C). The tiny distinction between cancer and normal cells is verified by other work as well, and it is mainly put down to the fact that cancer cells need more glucose to make up for their anaerobic respiration.[49] Besides, *in vitro* monitoring of ATP variation is implemented by using oligomycin (a kind of ATPase inhibitor decreasing ATP content)[48] and $CaCl_2$ (up-regulate ATP content)[49] as the modulation media for the A549 cell, respectively. Compared with the untreated group, the ATP


https://dx.doi.org/10.1021/acsnano.0c09986
ACS Nano XXXX, XXX, XXX−XXX

content of oligomycin treated group falls to 2.71 mM/cell ($P < 0.01$) while the up-regulated group rises to 8.35 mM/cell ($P < 0.01$, Figure 5D).

**On-Site Detection of $Na^+$ in Human Plasma.** Ascribing to the function of balancing pH and osmotic pressure, sodium is one of the most essential trace elements in human body fluids.[50,51] For clinical practice, the normal $Na^+$ level in plasma should be retained between 135 and 145 mM; otherwise, various physical symptoms such as headache and weakness may happen to hyponatremia patients (HPs, $Na^+$ level <135 mM).[51] Generally, the $Na^+$ meter is easily disturbed by environmental fluctuations, and it is desirable to construct a more stable assay approach. To this end, the on-site detection of $Na^+$ level in real human plasma samples is performed. Considering many interfering matrices in such challenging biological medium can produce underlying background signals, the S/B ratio should be first determined in this complex environment. Fortunately, due to the strong anti-interference merit originating from the upconversion luminescence based signal readout, no noticeable autofluorescence and scattering light come to our method even in whole plasma (the S/B ratio is at the same level to the buffer solution, Figure S14). After collecting the venous bloods (whole bloods) from 36 cases of HPs and 12 cases of healthy donors (HDs) and centrifuging to obtain their yellow whole plasmas (Figure 5E), the diluted samples are analyzed by the same way. The results in Figure 5F clearly manifest that our method is able to distinguish the different $Na^+$ levels between HPs and HDs. In addition, the calculated $Na^+$ levels for all cases are in good agreement with those assessed by $Na^+$ meter ($P > 0.05$, Figure 5G). Furthermore, the area under the curve (AUC) of our method presented in the receiver operating characteristic (ROC) curve is almost equal to that of $Na^+$ meter (AUCs are 0.962 and 0.943, respectively), suggesting a high assay accuracy for clinical samples.

## CONCLUSIONS

In this study, we have integrated some additional concepts to develop a special CRISPR/Cas12a biosensor. Since fDNAs are able to specifically identify a wide range of targets, the sensing coverage is effectively extended to other non-nucleic acid analytes such as ATP and $Na^+$ by severally using aptamer and DNAzyme to accurately transduce. In the presence of these model analytes, the CRISPR/Cas12a system can work as an efficient signal actuator to be successfully activated and the expected *trans*-cleave effect is as efficient as the pure CRISPR/Cas12a case. After performing the transduction modes on a bead interface, the target analytes can be well enriched. For such a bead-supported imaging platform, the fluid disturbance is entirely avoided *via* forceful holographic optical tweezers, by which we can form a fairly stable 3 × 3 bead array in three dimensions, providing a favorable imaging condition to enhance detection flux. Furthermore, a rational sandwich structure is fabricated to construct an energy-concentrating UCNP donor by perfectly restricting the luminescence domain into an extremely narrow space scope (2.09 nm), endowing not only a robust working adaptation in complicated biological samples but also a very high LRET efficiency (96.1%) to the surface acceptors. Based on the proposed improving routes, the accuracy-enhanced assay approach demonstrated here shows quite satisfactory sensitivity toward ATP and $Na^+$ (the LODs are as low as 87 pM and 4.3 nM, respectively) and superior specificity. Most importantly, the method can accurately measure the ATP content in single cell and the $Na^+$ level in body fluid, offering a prospective diagnostic technique for medical laboratory. Its future development will concentrate on introducing advanced trapping manners to realize higher flux analysis and exploring approximate pathways to analyze other important biomolecules.

## EXPERIMENTAL SECTION

**Synthesis of OA-Coated $NaYF_4$ (OA-core).** A 21 mL portion of OA/ODE (v/v = 2:5) mixed solvent was first added into a 100 mL three-neck round-bottom flask containing 1 mmol of $YCl_3{\cdot}6H_2O$ and then fully stirred together for 5 min. Next, the flask was vacuum treated using an oil pump for at least 30 min until no bubbles appeared in the solution. After the slurry was heated to 150 °C to form a homogeneous system under high-purity Ar atmosphere, the yellowish solution was allowed to cool to room temperature and further injected dropwise with 10 mL of freshly prepared methanol mixture containing 6.5 mmol of $NaOH/NH_4F$ (molar ratio = 2.5:4), followed by vigorously stirring the white cloudy oleate intermediates for 20 min. Subsequently, the system was kept at 120 °C for degrassing to completely evaporate off the needless methanol and other impurities with low boiling points as well as residual oxygen until a clear solution was presented again. Thereafter, the reaction temperature was rapidly increased to 300 °C (heating rate is ∼20 °C/min) with gentle stirring under Ar flow for 60 min. Once excess ethanol was added into the cooled flask to precipitate out the products from the golden yellow solution, the resultant nanoparticles were evenly divided into several 5 mL tubes and collected by centrifuging at 12000 rpm for 3 min. Then, each aliquot was washed several times in turn with ethanol/water (v/v = 1:1) and ethanol/cyclohexane (v/v = 6:1) mixed solvents to remove the remaining inorganic and organic reactants, respectively. By combining the purified nanoparticles, the final products were dispersed into 8 mL of chloroform *via* ultrasonic processing for 3 min (concentration is ∼10 mg/mL, stored at 4 °C).

**Development of OA-Coated Inner Shell on OA-Core (OA-Core−Shell).** First, a mixture (0.25 mmol) of rare earth chloride hydrates in a specified proportion (80% Y, 18% Yb, 2% Er) was added into a 50 mL three-neck round-bottom flask containing 3 mL of OA and 7.5 mL of ODE. After adequate handling by vacuum processing and vigorously stirring the slurry to turn into a clear solution at 150 °C, the flask was cautiously injected with the previously retrieved OA-core chloroform solution and further degassed at 120 °C to evaporate off the needless chloroform. Then 5 mL of freshly prepared methanol solvent dissolved with 6.5 mmol of $NaOH/NH_4F$ (molar ratio = 2.5:4) was added dropwise into the system to obtain the slightly turbidity intermediates, followed by degassing at 120 °C for 10 min and heating to 300 °C within 20 min. By maintaining gentle stirring at this warm temperature under Ar atmosphere for 20 min to form a yellowish homogeneous solution, the products were precipitated out by mixing with excess ethanol at room temperature. Finally, following the same washing and purification procedures, the collected products were dispersed into 8 mL of chloroform (concentration is ∼10 mg/mL, stored at 4 °C).

**Development of OA-Coated Outer Shell on OA-Core−Shell (OA-SUCNP).** A 10.5 mL portion of OA/ODE (v/v = 2:5) mixed solvent was first added into a 50 mL three-neck round-bottom flask containing 0.25 mmol of $YCl_3{\cdot}6H_2O$ and then treated with vacuum processing under vigorous stirring. After that, the flask temperature was increased to 150 °C until the slurry becomes clear under Ar flow. Next, the system was carefully injected with the earlier collected OA-core−shell chloroform solution and further degrassed at 120 °C for 15 min, followed by mixing with 5 mL of freshly prepared methanol solvent containing 6.5 mmol of $NaOH/NH_4F$ (molar ratio = 2.5:4). By further degrassing and rapidly heating to 300 °C, the flask was allowed to maintain the warm and Ar atmosphere for 20 min under gentle stirring. Once the flask was cooled to room temperature, the yellowish solution was fully stirred together with adequate ethanol. The precipitated products were washed and collected in sequence, and finally treated with ultraphonic to disperse into 8 mL of chloroform (concentration is ∼10 mg/mL, stored at 4 °C). To effectively regulate the thickness of


https://dx.doi.org/10.1021/acsnano.0c09986
ACS Nano XXXX, XXX, XXX−XXX

outer shell, different ratios of OA/ODE can be introduced in this shell development process.

**Surface PAA Modification of SUCNP (PAA-SUCNP).** A 1000 mg of PAA was first fully dissolved into 30 mL of DEG to form a transparent solution and then transferred to a 100 mL three-neck round-bottom flask. Thereafter, the system was processed with vacuum treatment for 40 min, followed by adding dropwise with the earlier dispersed OA-SUCNP chloroform solution. By degassing at 100 °C for at least 30 min to completely evaporate off the chloroform, the solution temperature was increased to 250 °C as quickly as possible and continued to stir gently for 120 min under Ar atmosphere. After mixing with 30 mL of acetone to precipitate out the products at room temperature, the nanoparticles collected by high speed centrifugation (18000 rpm) were washed five times with ethanol and dispersed into 8 mL of ultrapure water *via* ultrasonic processing for 5 min (concentration is ~10 mg/mL, stored at 4 °C for long-term usage).

**Covalent Assembly of ASB and PAA-SUCNP.** Initially, 5 μL of original ASB suspension was centrifuged at 5000 rpm for 3 min in a 1.5 mL tube and further washed three times with ultrapure water. After orderly redispersing the suspension into 100 μL of MES buffer solution (25 mM, pH 6.5) and mixing with 20 μg of PAA-SUCNP *via* ultrasonic treatment, 4 μL of 10 mg/mL EDC solution (freshly prepared) was introduced into the mixture. Upon gently incubating for 60 min in an oscillator at 30 °C, 80 μg of EDC was additionally supplied into the tube to maintain the activating reaction for 240 min. Next, the residual PAA-SUCNPs were removed by centrifugating at 5000 rpm for 6 min. By washing the assembled ASBs with ultrapure water containing 0.5% Tween 20 for three times, the resulting products were resuspended into 150 μL of MES buffer solution for further use (stored at 4 °C).

**Covalently Conjugating Reporter.** The as-obtained PAA-SUCNP assembled ASB suspension was first mixed together with 4 μL of 1 μM reporter *via* vortex in a 1.5 mL tube and then provided with 50 μL of MES buffer solution. After addition of 2 μL of 10 mg/mL EDC solution (freshly prepared), the tube was transferred to an oscillator and incubated at 30 °C for 60 min. Subsequently, the system was introduced with 10 μg of EDC, followed by maintaining the incubation for 60 min. Finally, centrifugal washing procedures with ultrapure water containing 0.5% Tween 20 were performed to remove the unconjugated reporters and the reporters conjugated ASBs was resuspended into 200 μL of reaction buffer solution (50 mM Tris-base, pH 8.0, 10 mM $MgCl_2$, 0.1 mg/mL BSA).

**Preparation of Cas12a-CrRNA Complex.** A 100 μL portion of 1 μM CrRNA and 200 μL of 1 μM Lbcas12a were incubated in a 1.5 mL RNase-free tube at 37 °C for 10 min.

**Quantitative Analysis of Standard ATP in Buffer Solution.** First, a 1.5 mL tube was orderly added with 2.5 nmol of activator, 5 nmol of aptamer 1, and 5 nmol of aptamer 2 and provided with 100 μL of reaction buffer solution. By fully mixing the mixture *via* vortex, the tube was placed in a 95 °C water bath and maintained at that temperature for 10 min. Then the heated tube was immediately transferred to a −20 °C refrigerator and cooled for 15 min, followed by evenly dividing the mixture into 10 1.5 mL RNase-free tubes. Next, various amounts of ATP (0 pmol, 0.01 pmol, 0.05 pmol, 0.1 pmol, 0.5 pmol, 1 pmol, 5 pmol, 0.01 nmol, 0.05 nmol, 0.2 nmol) were introduced separately into each tube and continued to incubate gently at 42 °C for 30 min. After addition of 10 μL of Cas12a-CrRNA complex and 20 μL of reporter conjugated ASB suspension, each tube was provided with a certain amount of reaction buffer solution to maintain its final volume at 100 μL. By continuing the incubation at 37 °C for 15 min, the resulting beads were washed three times with ultrapure water containing 0.5% Tween 20 and resuspended into 100 μL of reaction buffer solution. For holographic optical tweezers assisted imaging detection, 10 bead array images were measured for each testing group under an exposure time of 400 ms.

**Quantitative Detection of Standard $Na^+$ in Buffer Solution.** A 2.5 nmol solution of of $Na^+$-dependent DNAzyme and 2.5 nmol of substrate was first mixed together in a 1.5 mL tube *via* vortex and then treated with annealing at 95 °C, followed by even dividing into 10 1.5 mL RNase-free tubes. Subsequently, various amounts of NaCl (0 pmol, 0.3 pmol, 0.8 pmol, 3 pmol, 8 pmol, 0.03 nmol, 0.08 nmol, 0.3 nmol, 3 nmol) was introduced separately into each tube and continued gently incubating at 37 °C for 15 min. Subsequently, 10 μL of Cas12a-CrRNA and 20 μL of reporters conjugated ASB suspension were added into each tube and further provided with certain amounts of reaction buffer solution to keep their final volumes at 100 μL. After maintaining the incubation at 37 °C for 15 min and performing the washing process, the quantitative detection was same as the ATP analysis.

## ASSOCIATED CONTENT

### Supporting Information

The Supporting Information is available free of charge at https://pubs.acs.org/doi/10.1021/acsnano.0c09986.

Reagents, blood samples, instrumentation, fabrication of self-made PDMS chamber, calibration of optical tweezers setup, specificity examinations for ATP and $Na^+$, cell culture, quantitative analysis in real samples including single cell lysates and human plasma, size statistical data of UCNPs, high-resolution TEM images of UCNPs, digital images of UCNPs, upconversion luminescence mechanism of SUCNP, stability investigation of PAA-SUCNP, UV spectra and Zeta potential before and after conjugating with reporters, TEM images and size statistical data of SUCNPs with thicker outer shells, XRD patterns and FT-IR spectra of SUCNPs with larger sizes, optimal collateral cleavage reaction conditions for CRISPR/Cas12a system, investigation of $Na^+$-dependent DNAzyme, comparison of S/B ratios, and Tables S1−S4 (PDF)

## AUTHOR INFORMATION


### Corresponding Authors

**Cheng-Yu Li** − *Hubei Province Key Laboratory of Occupational Hazard Identification and Control, School of Public Health, Medical College, Wuhan University of Science and Technology, Wuhan 430065, People's Republic of China;* orcid.org/0000-0003-4463-717X; Email: li-chengyu@wust.edu.cn

**Hong-Wu Tang** − *Key Laboratory of Analytical Chemistry for Biology and Medicine (Ministry of Education), College of Chemistry and Molecular Sciences, Wuhan University, Wuhan 430072, People's Republic of China;* orcid.org/0000-0002-2258-6992; Email: hwtang@whu.edu.cn

### Authors

**Bei Zheng** − *Key Laboratory of Analytical Chemistry for Biology and Medicine (Ministry of Education), College of Chemistry and Molecular Sciences, Wuhan University, Wuhan 430072, People's Republic of China*

**Jiang-Tao Li** − *Key Laboratory of Analytical Chemistry for Biology and Medicine (Ministry of Education), College of Chemistry and Molecular Sciences, Wuhan University, Wuhan 430072, People's Republic of China*

**Jia-ling Gao** − *Hubei Province Key Laboratory of Occupational Hazard Identification and Control, School of Public Health, Medical College, Wuhan University of Science and Technology, Wuhan 430065, People's Republic of China*

**Yu-Heng Liu** − *Hubei Province Key Laboratory of Occupational Hazard Identification and Control, School of Public Health, Medical College, Wuhan University of Science and Technology, Wuhan 430065, People's Republic of China*

**Dai-Wen Pang** − *State Key Laboratory of Medicinal Chemical Biology, Tianjin Key Laboratory of Biosensing and Molecular Recognition, Research Center for Analytical Sciences, and College of Chemistry, Nankai University, Tianjin 300071,*




https://dx.doi.org/10.1021/acsnano.0c09986
ACS Nano XXXX, XXX, XXX−XXX

*People's Republic of China;* orcid.org/0000-0002-7017-5725

Complete contact information is available at: https://pubs.acs.org/10.1021/acsnano.0c09986

### Notes

The authors declare no competing financial interest.

## ACKNOWLEDGMENTS

This work was supported by the National Natural Science Foundation of China (21904102, 81772256, and 21827808).

## REFERENCES

(1) Shan, Y. Y.; Zhou, X. M.; Huang, R.; Xing, D. High-Fidelity and Rapid Quantification of MiRNA Combining CrRNA Programmability and CRISPR/Cas13a Trans-Cleavage Activity. *Anal. Chem.* **2019**, *91*, 5278−5285.

(2) Li, Y.; Teng, X. C.; Zhang, K. X.; Deng, R. J.; Li, J. H. RNA Strand Displacement Responsive CRISPR/Cas9 System for mRNA Sensing. *Anal. Chem.* **2019**, *91*, 3989−3996.

(3) Liang, M. D.; Li, Z. L.; Wang, W. S.; Liu, J. K.; Liu, L. S.; Zhu, G. L.; Karthik, L.; Wang, M.; Wang, K. F.; Wang, Z.; Yu, J.; Shuai, Y. T.; Yu, J. M.; Zhang, L.; Yang, Z. H.; Li, C.; Zhang, Q.; Shi, T.; Zhou, L. M.; Xie, F.; et al. A CRISPR-Cas12a-Derived Biosensing Platform for the Highly Sensitive Detection of Diverse Small Molecules. *Nat. Commun.* **2019**, *10*, 3672.

(4) Dai, Y. F.; Somoza, R. A.; Wang, L.; Welter, J. F.; Li, Y.; Caplan, A. I.; Liu, C. C. Exploring the Trans-Cleavage Activity of CRISPR-Cas12a (cpf1) for the Development of a Universal Electrochemical Biosensor. *Angew. Chem., Int. Ed.* **2019**, *58*, 17399−17405.

(5) Zhang, D. C.; Yan, Y. R.; Que, H. Y.; Yang, T. T.; Cheng, X. X.; Ding, S. J.; Zhang, X. M.; Cheng, W. CRISPR/Cas12a-Mediated Interfacial Cleaving of Hairpin DNA Reporter for Electrochemical Nucleic Acid Sensing. *ACS Sensors* **2020**, *5*, 557−562.

(6) Yuan, C. Q.; Tian, T.; Sun, J.; Hu, M. L.; Wang, X. S.; Xiong, E. H.; Cheng, M.; Bao, Y. J.; Lin, W.; Jiang, J. M.; Yang, C. W.; Chen, Q.; Zhang, H.; Wang, H.; Wang, X. R.; Deng, X. B.; Liao, X. P.; Liu, Y. H.; Wang, Z.; Zhang, G. H.; et al. Universal and Naked-Eye Gene Detection Platform Based on the Clustered Regularly Interspaced Short Palindromic Repeats/Cas12a/13a System. *Anal. Chem.* **2020**, *92* (5), 4029−4037.

(7) Wang, X. S.; Xiong, E. H.; Tian, T.; Cheng, M.; Lin, W.; Wang, H.; Zhang, G. H.; Sun, J.; Zhou, X. M. Clustered Regularly Interspaced Short Palindromic Repeats/Cas9-Mediated Lateral Flow Nucleic Acid Assay. *ACS Nano* **2020**, *14*, 2497−2508.

(8) Hu, M. L.; Yuan, C. Q.; Tian, T.; Wang, X. S.; Sun, J.; Xiong, E. H.; Zhou, X. M. Single-Step, Salt-Aging-Free, and Thiol-Free Freezing Construction of AuNP-Based Bioprobes for Advancing CRISPR-Based Diagnostics. *J. Am. Chem. Soc.* **2020**, *142*, 7506−7513.

(9) Chen, Q.; Tian, T.; Xiong, E. H.; Wang, P.; Zhou, X. M. CRISPR/Cas13a Signal Amplification Linked Immunosorbent Assay for Femtomolar Protein Detection. *Anal. Chem.* **2020**, *92*, 573−577.

(10) Shen, J. J.; Zhou, X. M.; Shan, Y. Y.; Yue, H. H.; Huang, R.; Hu, J. M.; Xing, D. Sensitive Detection of a Bacterial Pathogen Using Allosteric Probe-Initiated Catalysis and CRISPR-Cas13a Amplification Reaction. *Nat. Commun.* **2020**, *11*, 267.

(11) Xiong, Y.; Zhang, J. J.; Yang, Z. L.; Mou, Q. B.; Ma, Y.; Xiong, Y. H.; Lu, Y. Functional DNA Regulated CRISPR-Cas12a Sensors for Point-of-Care Diagnostics of Non-Nucleic-Acid Targets. *J. Am. Chem. Soc.* **2020**, *142*, 207−213.

(12) Wang, D. X.; Wang, J.; Du, Y. C.; Ma, J. Y.; Wang, S. Y.; Tang, A. N.; Kong, D. M. CRISPR/Cas12a-Based Dual Amplified Biosensing System for Sensitive and Rapid Detection of Polynucleotide Kinase/Phosphatase. *Biosens. Bioelectron.* **2020**, *168*, 112556.

(13) Cong, L.; Ran, F. A.; Cox, D.; Lin, S. L.; Barretto, R.; Habib, N.; Hsu, P. D.; Wu, X. B.; Jiang, W. Y.; Marraffini, L. A.; Zhang, F. Multiplex Genome Engineering Using CRISPR/Cas Systems. *Science* **2013**, *339* (6121), 819−823.

(14) Dai, Y. F.; Wu, Y. F.; Liu, G. Z.; Gooding, J. J. CRISPR Mediated Biosensing Toward Understanding Cellular Biology and Point-of-Care Diagnosis. *Angew. Chem., Int. Ed.* **2020**, *59*, 20754−20766.

(15) Chen, J. S.; Ma, E. B.; Harrington, L. B.; Da Costa, M.; Tian, X. R.; Palefsky, J. M.; Doudna, J. A. CRISPR-Cas12a Target Binding Unleashes Indiscriminate Single-Stranded DNAse Activity. *Science* **2018**, *360*, 436−439.

(16) Gootenberg, J. S.; Abudayyeh, O. O.; Kellner, M. J.; Joung, J.; Collins, J. J.; Zhang, F. Multiplexed and Portable Nucleic Acid Detection Platform with Cas13, Cas12a, and Csm6. *Science* **2018**, *360*, 439−444.

(17) Leng, Y. K.; Sun, K.; Chen, X. Y.; Li, W. W. Suspension Arrays Based on Nanoparticle-Encoded Microspheres for High-Throughput Multiplexed Detection. *Chem. Soc. Rev.* **2015**, *44*, 5552−5595.

(18) Komnatnyy, V. V.; Nielsen, T. E.; Qvortrup, K. Bead-Based Screening in Chemical Biology and Drug Discovery. *Chem. Commun.* **2018**, *54*, 6759−6771.

(19) Fang, X. N.; Zheng, Y. Z.; Duan, Y. K.; Liu, Y.; Zhong, W. W. Recent Advances in Design of Fluorescence-Based Assays for High-Throughput Screening. *Anal. Chem.* **2019**, *91*, 482−504.

(20) Zhang, Z. M.; Shikha, S.; Liu, J. L.; Zhang, J.; Mei, Q. S.; Zhang, Y. Upconversion Nanoprobes: Recent Advances in Sensing Applications. *Anal. Chem.* **2019**, *91*, 548−568.

(21) Li, C. Y.; Zheng, B.; Kang, Y. F.; Tang, H. W.; Pang, D. W. Integrating 808 nm Light-Excited Upconversion Luminescence Powering with DNA Tetrahedron Protection: An Exceptionally Precise and Stable Nanomachine for Intracelluar MicroRNA Tracing. *ACS Sensors* **2020**, *5*, 199−207.

(22) Wen, S. H.; Zhou, J. J.; Zheng, K. Z.; Bednarkiewicz, A.; Liu, X. G.; Jin, D. Y. Advances in Highly Doped Upconversion Nanoparticles. *Nat. Commun.* **2018**, *9*, 2415.

(23) Drees, C.; Raj, A. N.; Kurre, R.; Busch, K. B.; Haase, M.; Piehler, J. Engineered Upconversion Nanoparticles for Resolving Protein Interactions inside Living Cells. *Angew. Chem., Int. Ed.* **2016**, *55*, 11668−11672.

(24) Muhr, V.; Wurth, C.; Kraft, M.; Buchner, M.; Baeumner, A. J.; Resch-Genger, U.; Hirsch, T. Particle-Size-Dependent Forster Resonance Energy Transfer from Upconversion Nanoparticles to Organic Dyes. *Anal. Chem.* **2017**, *89*, 4868−4874.

(25) Wang, G.; Fu, Y. K.; Ren, Z. H.; Huang, J.; Best, S.; Li, X.; Han, G. R. Upconversion Nanocrystal "Armoured" Silica Fibres with Superior Photoluminescence for MiRNA Detection. *Chem. Commun.* **2018**, *54*, 6324−6327.

(26) Gao, M. P.; Wu, R. Y.; Mei, Q. S.; Zhang, C. L.; Ling, X.; Deng, S. S.; He, H. B.; Zhang, Y. Upconversional Nanoprobes with Highly Efficient Energy Transfer for Ultrasensitive Detection of Alkaline Phosphatase. *ACS Sensors* **2019**, *4*, 2864−2868.

(27) You, Y.; Cheng, S. S.; Zhang, L.; Zhu, Y. X.; Zhang, C. L.; Xian, Y. Z. Rational Modulation of the Luminescence of Upconversion Nanomaterials with Phycocyanin for the Sensing and Imaging of Myeloperoxidase during an Inflammatory Process. *Anal. Chem.* **2020**, *92*, 5091−5099.

(28) Li, Z.; Lv, S. W.; Wang, Y. L.; Chen, S. Y.; Liu, Z. H. Construction of LRET-Based Nanoprobe Using Upconversion Nanoparticles with Confined Emitters and Bared Surface as Luminophore. *J. Am. Chem. Soc.* **2015**, *137*, 3421−3427.

(29) Zhang, X. B.; Chen, W. W.; Xie, X. Y.; Li, Y. Y.; Chen, D. S.; Chao, Z. C.; Liu, C. H.; Ma, H. B.; Liu, Y.; Ju, H. X. Boosting Luminance Energy Transfer Efficiency in Upconversion Nanoparticles with an Energy-Concentrating Zone. *Angew. Chem., Int. Ed.* **2019**, *58*, 12117−12122.

(30) Tanaka, Y.; Wakida, S. Time-Shared Optical Tweezers with a Microlens Array for Dynamic Microbead Arrays. *Biomed. Opt. Express* **2015**, *6*, 3670−3677.

(31) Zheng, B.; Kang, Y. F.; Zhang, T.; Li, C. Y.; Huang, S.; Zhang, Z. L.; Wu, Q. S.; Qi, C. B.; Pang, D. W.; Tang, H. W. Improving Flow Bead Assay: Combination of Near-Infrared Optical Tweezers Stabilizing and

Upconversion Luminescence Encoding. *Anal. Chem.* **2020**, *92*, 5258−5266.
(32) Ashkin, A.; Dziedzic, J. M.; Bjorkholm, J. E.; Chu, S. Observation of a Single-Beam Gradient Force Optical Trap for Dielectric Particles. *Opt. Lett.* **1986**, *11*, 288−290.
(33) Li, C. Y.; Cao, D.; Kang, Y. F.; Lin, Y.; Cui, R.; Pang, D. W.; Tang, H. W. Fluorescence Detection of H5N1 Virus Gene Sequences Based on Optical Tweezers with Two-Photon Excitation Using a Single Near Infrared Nanosecond Pulse Laser. *Anal. Chem.* **2016**, *88*, 4432−4439.
(34) Li, C. Y.; Cao, D.; Song, C. Y.; Xu, C. M.; Ma, X. Y.; Zhang, Z. L.; Pang, D. W.; Tang, H. W. Integrating Optical Tweezers with Up-Converting Luminescence: A Non-Amplification Analytical Platform for Quantitative Detection of MicroRNA-21 Sequences. *Chem. Commun.* **2017**, *53*, 4092−4095.
(35) Li, C. Y.; Kang, Y. F.; Qi, C. B.; Zheng, B.; Zheng, M. Q.; Song, C. Y.; Guo, Z. Z.; Lin, Y.; Pang, D. W.; Tang, H. W. Breaking through Bead-Supported Assay: Integration of Optical Tweezers Assisted Fluorescence Imaging and Luminescence Confined Upconversion Nanoparticles Triggered Luminescent Resonance Energy Transfer (LRET). *Anal. Chem.* **2019**, *91*, 7950−7957.
(36) Shaw, L. A.; Chizari, S.; Hopkins, J. B. Improving the Throughput of Automated Holographic Optical Tweezers. *Appl. Opt.* **2018**, *57*, 6396−6402.
(37) Bola, R.; Treptow, D.; Marzoa, A.; Montes-Usategui, M.; Martin-Badosa, E. Acousto-Holographic Optical Tweezers. *Opt. Lett.* **2020**, *45*, 2938−2941.
(38) Guo, H.; Li, Z. Q.; Qian, H. S.; Hu, Y.; Muhammad, I. N. Seed-Mediated Synthesis of $NaYF_4$:Yb, Er/$NaGdF_4$ Nanocrystals with Improved Upconversion Fluorescence and MR Relaxivity. *Nanotechnology* **2010**, *21*, 125602.
(39) Sedlmeier, A.; Gorris, H. H. Surface Modification and Characterization of Photon-Upconverting Nanoparticles for Bioanalytical Applications. *Chem. Soc. Rev.* **2015**, *44* (6), 1526−1560.
(40) Gabelica, V.; Rosu, F.; Tabarin, T.; Kinet, C.; Antoine, R.; Broyer, M.; De Pauw, E.; Dugourd, P. Base-Dependent Electron Photodetachment from Negatively Charged DNA Strands upon 260-nm Laser Irradiation. *J. Am. Chem. Soc.* **2007**, *129*, 4706−4713.
(41) Zhu, X. J.; Feng, W.; Chang, J.; Tan, Y. W.; Li, J. C.; Chen, M.; Sun, Y.; Li, F. Y. Temperature-Feedback Upconversion Nanocomposite for Accurate Photothermal Therapy at Facile Temperature. *Nat. Commun.* **2016**, *7*, 10437.
(42) Kang, Y. F.; Zheng, B.; Li, C. Y.; Zhang, Z. L.; Tang, H. W.; Wu, Q. S.; Pang, D. W. Real-Time Monitoring of Temperature Variations around a Gold Nanobipyramid Targeted Cancer Cell under Photothermal Heating by Actively Manipulating an Optically Trapped Luminescent Upconversion Microparticle. *Anal. Chem.* **2020**, *92*, 1292−1300.
(43) Gnanasammandhan, M. K.; Idris, N. M.; Bansal, A.; Huang, K.; Zhang, Y. Near-IR Photoactivation Using Mesoporous Silica-Coated $NaYF_4$:Yb,Er/Tm Upconversion Nanoparticles. *Nat. Protoc.* **2016**, *11*, 688−713.
(44) Nutiu, R.; Li, Y. F. Structure-Switching Signaling Aptamers. *J. Am. Chem. Soc.* **2003**, *125*, 4771−4778.
(45) Chen, K.; Huang, Q.; Fu, T.; Ke, G. L.; Zhao, Z. B.; Zhang, X. B.; Tan, W. H. MicroRNA-Initiated and Intracellular $Na^+$-Fueled DNAzyme Motor for Differentiating Molecular Subtypes of Nonsmall Cell Lung Cancer. *Anal. Chem.* **2020**, *92*, 7404−7408.
(46) Tsujimoto, Y. Apoptosis and Necrosis: Intracellular ATP Level as a Determinant for Cell Death Modes. *Cell Death Differ.* **1997**, *4*, 429−434.
(47) Gourine, A. V.; Llaudet, E.; Dale, N.; Spyer, K. M. ATP Is a Mediator of Chemosensory Transduction in the Central Nervous System. *Nature* **2005**, *436*, 108−111.
(48) Hong, S. N.; Zhang, X. T.; Lake, R. J.; Pawel, G. T.; Guo, Z. J.; Pei, R. J.; Lu, Y. A Photo-Regulated Aptamer Sensor for Spatiotemporally Controlled Monitoring of ATP in the Mitochondria of Living cells. *Chem. Sci.* **2020**, *11*, 713−720.
(49) Wang, D. D.; Qi, G. H.; Zhou, Y.; Zhang, Y.; Wang, B.; Hu, P.; Jin, Y. D. Single-Cell ATP Detection and Content Analyses in Electrostimulus-Induced Apoptosis Using Functionalized Glass Nanopipettes. *Chem. Commun.* **2020**, *56*, 1561−1564.
(50) Simpson, F. O. Sodium-Intake, Body Sodium, and Sodium-Excretion. *Lancet* **1988**, *2*, 25−29.
(51) Megahed, A. A.; Hiew, M.; Grunberg, W.; Trefz, F. M.; Constable, P. D. Evaluation of the Analytical Performance of a Portable Ion-Selective Electrode Meter for Measuring Whole-Blood, Plasma, Milk, Abomasal-Fluid, and Urine Sodium Concentrations in Cattle. *J. Dairy Sci.* **2019**, *102*, 7435−7444.


https://dx.doi.org/10.1021/acsnano.0c09986
*ACS Nano* XXXX, XXX, XXX−XXX